NeuroImage: Clinical 18 (2018) 996–1006

Contents lists available at ScienceDirect

NeuroImage: Clinical

journal homepage: www.elsevier.com/locate/ynicl

The site of stimulation moderates neuropsychiatric symptoms after subthalamic deep brain stimulation for Parkinson's disease

Philip E. Mosley[a,b,c,d,*], David Smith[a], Terry Coyne[c,e], Peter Silburn[b,c], Michael Breakspear[a], Alistair Perry[a,f]

[a] Systems Neuroscience Group, QIMR Berghofer Medical Research Institute, Herston, Queensland, Australia
[b] Neurosciences Queensland, St Andrew's War Memorial Hospital, Spring Hill, Queensland, Australia
[c] Queensland Brain Institute, University of Queensland, St Lucia, Queensland, Australia
[d] Faculty of Medicine, University of Queensland, Herston, Queensland, Australia
[e] Brizbrain and Spine, The Wesley Hospital, Auchenflower, Queensland, Australia
[f] Max Planck UCL Centre for Computational Psychiatry and Ageing Research, Berlin, Germany

ARTICLE INFO

Keywords:
Neuropsychiatry
Impulsivity
Parkinson's disease
Deep brain stimulation
Subthalamic nucleus

ABSTRACT

Deep brain stimulation of the subthalamic nucleus for Parkinson's disease is an established advanced therapy that addresses motor symptoms and improves quality of life. However, it has also been associated with neuropsychiatric symptoms such as impulsivity and hypomania. When significant, these symptoms can be distressing, necessitating psychiatric intervention. However, a comprehensive analysis of neurocognitive and neuropsychiatric outcomes with reference to the site of subthalamic stimulation has not been undertaken. We examined this matter in a consecutive sample of 64 persons with Parkinson's disease undertaking subthalamic deep brain stimulation. Participants were assessed with a battery of neuropsychiatric instruments at baseline and at repeated postoperative intervals. A psychiatrist identified patients with emergent, clinically-significant symptoms due to stimulation. The site of the active electrode contact and a simulated volume of activated tissue were evaluated with reference to putative limbic, associative and motor subregions of the subthalamic nucleus. We studied anatomical correlates of longitudinal neuropsychiatric change and delineated specific subthalamic regions associated with neuropsychiatric impairment. We tested the ability of these data to predict clinically-significant symptoms. Subthalamic stimulation within the right associative subregion was associated with inhibitory errors on the Excluded Letter Fluency task at 6-weeks ($p = 0.023$) and 13-weeks postoperatively ($p = 0.0017$). A cluster of subthalamic voxels associated with inhibitory errors was identified in the right associative and motor subregions. At 6-weeks, clinically-significant neuropsychiatric symptoms were associated with the distance of the active contact to the right associative subregion ($p = 0.0026$) and stimulation within the right associative subregion ($p = 0.0009$). At 13-weeks, clinically-significant symptoms were associated with the distance to the right ($p = 0.0027$) and left ($p = 0.0084$) associative subregions and stimulation within the right associative subregion ($p = 0.0026$). Discrete clusters of subthalamic voxels associated with high and low likelihood of postoperative neuropsychiatric symptoms were identified in ventromedial and dorsolateral zones, respectively. When a classifier was trained on these data, clinically-significant symptoms were predicted with an accuracy of 79%. These data underscore the importance of accurate electrode targeting, contact selection and device programming to reduce postoperative neuropsychiatric impairment. The ability to predict neuropsychiatric symptoms based on subthalamic data may permit anticipation and prevention of these occurrences, improving safety and tolerability.

1. Introduction

Subthalamic deep brain stimulation (DBS) is an advanced therapy for Parkinson's disease that reduces motor symptoms and improves quality of life (Schuepbach et al., 2013). However, the relationship between DBS and the neuropsychiatric features of Parkinson's disease is complex (Mosley and Marsh, 2015). Some individuals become more impulsive and less empathic after DBS, acting recklessly without foresight or concern for others. The incidence of this syndrome has been estimated at up to 15% (Appleby et al., 2007; Daniele et al., 2003).

* Corresponding author at: Neurosciences Queensland, Level 1, St Andrew's Place, 33 North Street, Spring Hill, Queensland 4000, Australia.
E-mail address: philip.mosley@qimrberghofer.edu.au (P.E. Mosley).

https://doi.org/10.1016/j.nicl.2018.03.009
Received 20 December 2017; Received in revised form 7 March 2018; Accepted 9 March 2018
Available online 13 March 2018

Predicting those persons who will develop this behavioural syndrome is a challenge for the clinician, given the wide spectrum of neuropsychiatric symptoms associated with PD (Weintraub and Burn, 2011). Furthermore, the predictive value of preoperative neuropsychiatric symptoms is unclear.

The emergence of postoperative impulsivity may be a neurostimulatory phenomenon related to the computational role of the STN in behaviour. In addition to its role as a relay nucleus that increases the inhibitory drive of the basal ganglia, the STN is a second input station to the basal ganglia, receiving direct cortical projections from the frontal lobe in the 'hyperdirect' pathway (Nambu et al., 2002). Here, the STN may 'brake' or 'delay' cognitive-associative circuits in the basal ganglia, suppressing impulsive and potentially error-prone responding. Functional and structural brain imaging support the role of this pathway in motor inhibition (Aron et al., 2007; Rae et al., 2015). Following STN DBS, persons with Parkinson's disease demonstrate failures of motor inhibition (Hershey et al., 2004), action cancellation, (Obeso et al., 2013), as well as showing a failure of prepotent verbal inhibition (Thobois et al., 2007; Witt et al., 2004). Furthermore, when faced with a difficult choice, persons with Parkinson's disease speed rather than slow their decision-making after STN-DBS (Cavanagh et al., 2011; Frank et al., 2007), where taking more time would be an optimal response in order to make an accurate decision. However, impulsivity is not the only behavioural symptom that has been reported subsequent to STN-DBS. Previous work has identified relationship discord precipitated by indifference to the emotional wellbeing of the partner of the person with Parkinson's disease (Lewis et al., 2015; Schupbach et al., 2006). One recent investigation has suggested a role for the STN in object valuation, which offers a potential mechanism for these more complex changes (Seymour et al., 2016).

The anatomy of the STN confers vulnerability to stimulation-dependent neuropsychiatric changes. A tripartite functional organization of the STN into limbic, associative and motor subregions is suggested by primate and human studies (Haynes and Haber, 2013; Lambert et al., 2012), although with considerable topological overlap and without lobar boundaries (Alkemade and Forstmann, 2014; Lambert et al., 2015). Yet, the small size of the STN means that current diffusion from a stimulating contact in the dorsolateral sensorimotor region could modulate subthalamic regions with greater connectivity to fronto-striatal networks implicated in mood, decision-making and reward. The more ventral and medial the stimulating contact, the more likely these circuits are to be affected by DBS. Accordingly, moving stimulation between active contacts in the dorsal motor and ventral limbic aspects of the nucleus can impair response inhibition (Hershey et al., 2010) and precipitate manic symptoms (Mallet et al., 2007). One investigation has examined the influence of electrode position on psychiatric outcomes in a sample larger than a small case series (Welter et al., 2014). Here, the depth of the active contact in both the right and left hemispheres, relative to the inter-commissure plane, was associated with postoperative hypomania. However, this investigation only included one formal postoperative assessment after 1 year, at which time only depressive symptoms were evaluated. Other psychiatric symptoms, including measures of impulsive responding, were not assessed.

The locus of subthalamic stimulation has been shown to affect motor outcomes after DBS for Parkinson's disease. Accurate targeting of the stimulating contact to the lateral aspect of the STN significantly improves motor symptoms (Wodarg et al., 2012). Recently, Akram et al. (2017) modelled the extent of neural tissue activation in the subthalamic region and regressed these against motor outcomes, delineating discrete clusters of subthalamic and peri-subthalamic voxels associated with maximal improvement in tremor, rigidity and bradykinesia. These were distributed in the posterior and superior aspects of the nucleus.

The aim of our investigation was to identify if the locus of subthalamic stimulation moderates the evolution of postoperative neuropsychiatric symptoms. Tractographic parcellation of the STN into motor, associative and limbic regions furnished precise information on the position of each electrode contact relative to these STN subregions. We simulated a volume of activated tissue (VAT) for each hemisphere, for each participant, at each follow up. This enabled us to estimate the dispersion of charge within each STN subregion at a given time, and allowed us to evaluate the contribution of stimulation parameters to emergent symptoms during titration. Finally, we applied these data to delineate STN regions significantly associated with neuropsychiatric impairment and tested the predictive validity of our data. Our hypotheses were that the position of the active electrode contact and dispersion of charge in the associative and limbic regions of the STN would be significant determinants of postoperative neuropsychiatric symptoms in individuals with Parkinson's disease.

2. Materials and methods

2.1. Participants

Sixty-four participants were consecutively recruited at the Asia-Pacific Centre for Neuromodulation between 2013 and 2017, during the assessment of eligibility for STN-DBS. The diagnosis of Parkinson's disease was confirmed according to the United Kingdom Queens Square Brain Bank criteria (Hughes et al., 1992). The laterality of disease onset and the Hoehn and Yahr stage (Hoehn and Yahr, 1967) at operation was recorded. The PD subtype (tremor-dominant, akinetic-rigid, mixed-type) was established based on an analysis of the dominant symptoms elicited during the Unified Parkinson's Disease Rating Scale (UPDRS) Part III Motor Examination, as described in Spiegel et al. (2007). Candidates with cognitive impairment were excluded, as defined by a Mini Mental State Examination Score (MMSE) of 25 or less or a clinical diagnosis of PD dementia. The latter was defined according to published Movement Disorder Society criteria (Emre et al., 2007). All participants completed a psychiatric and cognitive evaluation prior to surgery.

2.2. Image acquisition

A preoperative T1-weighted MPRAGE and a T2-weighted FLAIR sequence were acquired. For participants 1–26, this took place using a 3 T GE Signa Hdx with a 32-channel head coil at St Andrews War Memorial Hospital. The acquisition parameters were as follows: T1: 1 mm^3 voxel-resolution, TR = 6.13 ms, TE = 2.01 ms, flip angle = 15°, matrix size = 256 × 256, FOV = 256 × 256 × 166; T2: 1 × 1 × 2 mm voxel-resolution, TR = 9502 ms, TE = 120.54 ms, flip angle = 90°, matrix size = 256 × 256, FOV = 256 × 256 × 75. Participants 27–64 were scanned using a 3 T Siemens Prisma, with a 64-channel head coil at the Herston Imaging Research Facility. The acquisition parameters were as follows: T1, 1 mm^3 voxel-resolution, TR = 2000 ms, TE = 2.38 ms, flip angle = 9°, matrix size = 256 × 256, FOV = 256 × 256 × 192; T2, 1 × 1 × 2 mm voxel-resolution, TR = 9500 ms, TE = 122.0 ms, flip angle = 120°, matrix size = 256 × 256, FOV = 256 × 256 × 70. Postoperative CT images for all participants were acquired on a Siemens Intevo, with a resolution of 0.5 mm^3.

2.3. Surgery and clinical follow-up

Bilateral implantation of Medtronic 3389 (n = 48) or Boston Vercise (n = 16) electrodes took place in a single-stage procedure using a Leksell stereotactic apparatus, with the STN having been identified as a midbrain structure on Fluid Attenuation Inversion Recovery (FLAIR) imaging. Intraoperative microelectrode recordings (MER) were employed to establish localisation within the STN and intraoperative test stimulation was performed. A CT scan confirmed satisfactory postoperative lead placement. Contact selection for initial stimulation was based upon MER signals, with titration and evaluation of stimulation over the following week as an inpatient until motor symptoms were

satisfactorily treated without adverse effects. All implanted electrode contacts were of the ring rather than segmented configuration and thus no current-steering was applied. Post-discharge, participants returned to the movement disorders clinic for further neurological and psychiatric evaluation, with further DBS manipulation according to a set schedule of visits. The predominant criterion for DBS manipulation at each visit was manifest motor symptoms of Parkinson's disease. However, if the patient, caregiver or clinician detected neuropsychiatric symptoms (such as mood elevation, disinhibition or irritability) then a psychiatric review was initiated. Manipulation of the DBS device occurred immediately if neuropsychiatric symptoms were determined to be stimulation-related and clinically-significant (e.g. precipitating interpersonal impairment). All participants received routine psychiatric follow up as part of multidisciplinary care.

2.4. Neuropsychiatric outcomes

2.4.1. Neuropsychiatric assessments

Assessments took place prior to DBS and subsequently at 2-weeks, 6-weeks, 13-weeks and 26-weeks postoperatively, using the same battery of participant, caregiver and clinician-rated instruments, described in Mosley et al. (2018). This investigation focussed on neuropsychiatric symptoms identified as significant drivers of caregiver burden in a multivariate analysis (Mosley et al., 2018). Briefly, these included measures of *impulsivity*: the Barratt Impulsiveness Scale II (BIS) (Patton et al., 1995); the Questionnaire for Impulsive-Compulsive disorders in PD Rating Scale (QUIP-RS) (Weintraub et al., 2012); the Excluded Letter Fluency task (ELF) (Shores et al., 2006); the Hayling test (Burgess et al., 1997); *empathy*: the Empathy Quotient (EQ) (Baron-Cohen and Wheelwright, 2004); and *depression*: the Beck Depression Inventory II (BDI) (Beck et al., 1961). In addition, a modified version of the BIS and EQ (caregiver-rated BIS and caregiver-rated EQ) assessed these behaviours from the perspective of the caregiver, given that participant and caregiver ratings may be discrepant (Lewis et al., 2014).

Furthermore, at each visit motor symptoms were assessed with the UPDRS Part III motor examination. Dopaminergic medication was converted to a levodopa-equivalent daily dose (LEDD) value (Evans et al., 2004). DBS parameters such as active contacts, amplitude, pulsewidth, frequency and impedance were recorded. Participants with Boston electrodes (n = 16) had their stimulation amplitude converted from milliamps to volts using impedance measurements at the active contact. Participants were 'ON' medication and stimulation for all assessments, in order to provide a naturalistic evaluation of symptom evolution.

2.4.2. Neuropsychiatric 'caseness'

In addition to the above instruments, participants were assigned to the category 'case' or 'non-case' depending on whether they developed clinically-significant neuropsychiatric symptoms attributable to DBS, necessitating device manipulation (hereafter referred to as 'caseness'). This category was operationalised as follows: a participant was brought to the attention of the psychiatrist (who had assessed all participants at baseline) through self-referral, or via a relative or a clinician with concerns about the participant's mood or behaviour. The psychiatrist conducted a semi-structured diagnostic interview and mental state examination with attention to euphoria, irritability, disinhibition, impulsivity, compulsivity and empathy. If the psychiatrist considered that a stimulation-related neuropsychiatric presentation was likely and was causing clinically-significant impairment or distress, the neurologist adjusted the participant's DBS settings by moving to a new active contact or reducing the amplitude of stimulation. The psychiatrist then repeated the clinical assessment and sought collateral information from the participant's relatives. If the neuropsychiatric symptoms responded immediately to device manipulation then the participant was defined as a case.

A timeline displaying the sequence of assessments is presented in Fig. 1A.

2.5. Image processing

Preoperative MPRAGE and FLAIR images were co-registered with the postoperative CT scan using an affine transformation within FSL (FLIRT version 6.0, (Smith et al., 2004)). Each co-registration was manually checked for accuracy (Fig. 2A).

The co-registered acquisitions were spatially normalized into ICBM_2009b nonlinear asymmetric space using a fast diffeomorphic image registration algorithm (DARTEL) as implemented in SPM12 (Ashburner, 2007) (Fig. 2B and C). Using the Lead-DBS toolbox (version 1.6.4.2 (Horn and Kuhn, 2015)), (http://www.lead-dbs.org), electrodes were manually localised and corrected for brainshift by applying a refined affine transform calculated between pre- and postoperative acquisitions (Fig. 2E). A volume of activated tissue (VAT), representing the dispersion of electrical charge in neural tissue, was estimated based upon individualised stimulation parameters (Madler and Coenen, 2012) at each assessment interval (Fig. 2F).

The spatial position of each electrode contact was evaluated with reference to a tractrographic parcellation of the STN into *limbic*, *associative* and *motor* subregions (Accolla et al., 2014). For both hemispheres we calculated: 1) the distance of the electrode contact to the centroid of each STN subregion; 2) the distance to the nearest voxel of that volume; and 3) extent of each subregion volume occupied by each participant's simulated VAT. These variables are detailed in Table 1. The image processing pipeline is depicted in Fig. 2. Code supporting these workflows is publically available at https://github.com/AlistairPerry/DBSVATstats. Images were projected onto the BigBrain histological atlas for visualisation purposes (Amunts et al, 2013).

2.6. Statistical analysis

The emphasis of this investigation was on emergent neuropsychiatric symptoms attributable to subthalamic stimulation. By week 26, any emergent neuropsychiatric symptoms linked to stimulation had attenuated following clinical intervention. No participants in this cohort became a 'case' between the 13 and 26-week assessment. The assessment at week 2 was discounted as residual lesion effects from electrode implantation could not be excluded. Therefore, the focus of this analysis was the assessments at 6 and 13-weeks, relative to baseline.

At each assessment interval, data was z-normalized to account for the heterogeneity of and variance in assessment instruments. To calculate the rates of change for each neuropsychiatric outcome, normalized scores at baseline were subtracted from each follow-up assessment. Across the complete data set, < 0.03% was missing for any variable. Missing data was inferred using the pooled results of 50 iterations of longitudinal imputation by classification and regression trees, employing Gibbs sampling using *mice* in the R software environment. (R Core Team, 2014; van Buuren and Groothuis-Oudshoorn, 2011). The distribution of original and imputed data was checked for plausibility and results are displayed in Supplementary Fig. 1. At baseline and during follow up, the demographic and phenotypic characteristics of those participants who would become postoperative cases were contrasted with non-cases. Data with a non-Gaussian distribution was treated with the Kruskal-Wallis test. The Chi-squared test was employed for categorical variables. Prior to variable selection, a repeated-measures analysis of variance (ANOVA) was first employed to identify significant group-level longitudinal changes in neuropsychiatric assessment data. When multiple comparisons were undertaken, reported *p*-values were adjusted using the Benjamini and Hochberg (1995) method to control for the false discovery rate, with $\alpha = 0.05$.

2.6.1. Variable selection and modelling

To reduce the dimensionality of the dataset, comprising of many candidate anatomical and neuropsychiatric covariates, resolve

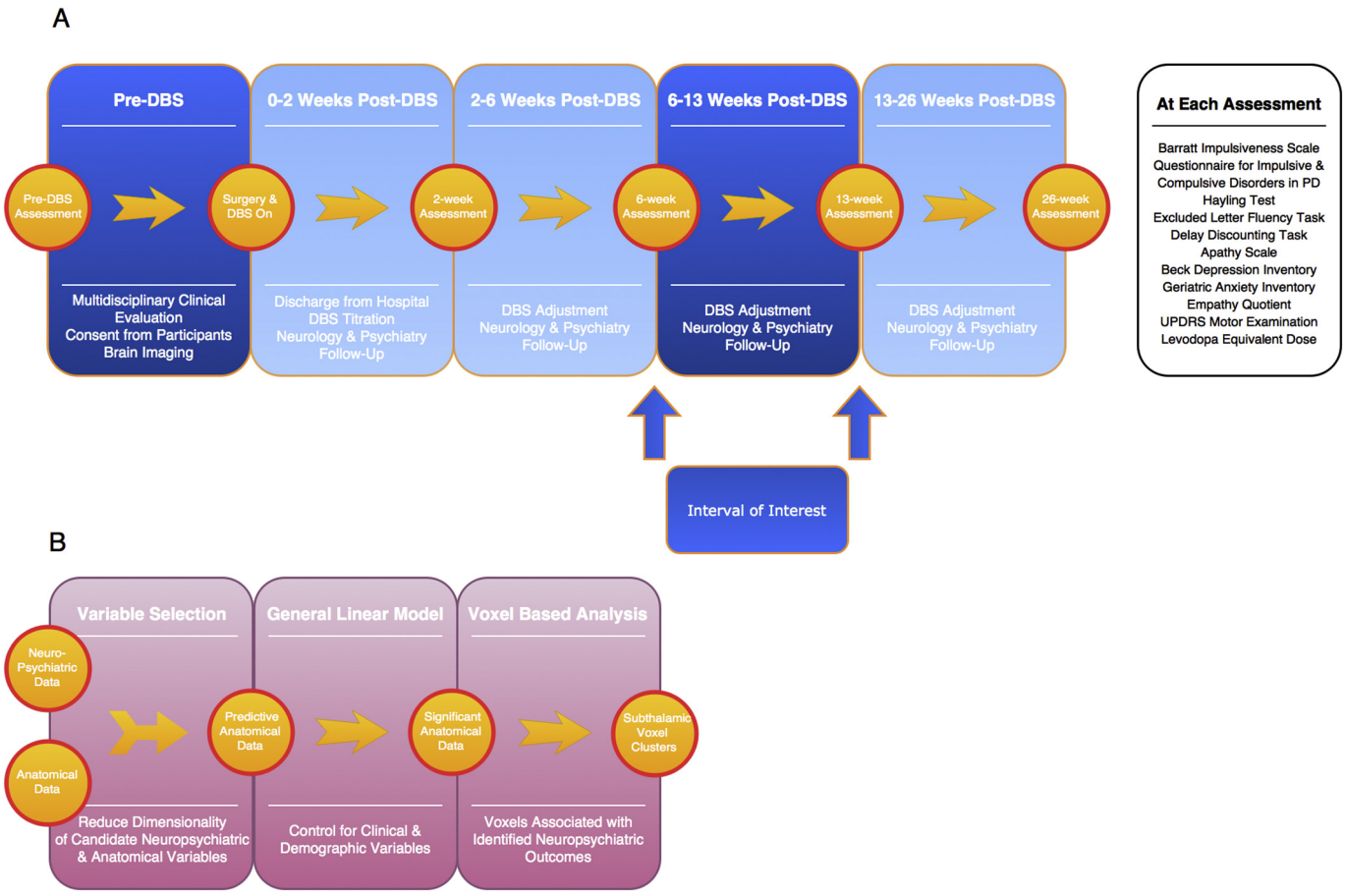

Fig. 1. A: Timeline of participant assessments during the investigation. All participants underwent a multidisciplinary assessment at baseline prior to DBS, which included a psychiatric assessment. Participants also undertook a battery of neuropsychiatric instruments prior to DBS and at four postoperative intervals. Between postoperative assessments, participants received standard neurology and psychiatry follow up, with surveillance for the evolution of clinically-significant neuropsychiatric symptoms attributable to DBS. The interval of interest for this investigation was between the assessments at 6 and 13-weeks post-DBS. B: Statistical flowchart illustrating the modelling of candidate neuropsychiatric and anatomical variables, controlling for disease and demographic factors, following by the identification of subthalamic voxel clusters significantly associated with neuropsychiatric impairment.

unknown dependencies and remove redundant variables, a variable selection and regularisation algorithm (the Least Absolute Shrinkage and Selection Operator: LASSO) was employed to identify the combination of anatomical variables with the best predictive value for each neuropsychiatric outcome (Friedman et al., 2010). A conservative one-standard-deviation rule was chosen for the regularisation parameter (λ) to protect against overfitting (Hastie et al., 2009). A binary model was employed for binary outcomes, a Gaussian model for parametric data and a Poisson model for nonparametric data.

Subsequently, neuropsychiatric variables and their anatomical predictors as identified from the LASSO were modelled in a general linear model, with the model family defined by the nature of the dependent variable. Demographic and disease-related factors, including change in LEDD, were also entered as covariates. These analyses also took place in the R software environment, using *glmnet* for optimisation and *glm* for general linear modelling. A schematic of these steps is presented in Fig. 1B. Scanning site was included as a covariate for all significant effects (Supplementary Table 8).

2.6.2. Subthalamic voxels associated with neuropsychiatric symptoms

In order to extend the findings from the general linear model, spatial clusters of subthalamic voxels associated with the neuropsychiatric outcomes were identified using threshold-free cluster-enhancement (TFCE) (Smith and Nichols, 2009). Here, hemispheric VATs for all participants at the intervals of interest were first concatenated into a 4-dimensional image and overlapping voxels within this image were thresholded to verify that the highest probability of stimulation was within the atlas-defined STN (Accolla et al., 2014). Each voxel within this defined STN mask was entered into a general linear model against the demeaned neuropsychiatric outcome scores – with the TFCE used as the test-statistic. Using FSL *Randomise* (Winkler et al., 2014), non-parametric permutation inference was then conducted upon each voxel to control for family-wise error (FWE), employing 5000 permutations to build up the null distribution. Voxels significantly associated with neuropsychiatric outcome of interest were identified by $\alpha = 0.05$ (FWE-corrected). FSL *Cluster* was employed for cluster-based inference and local maxima extraction.

2.6.3. Classification of clinically-significant symptoms

Finally, the ability of these anatomical data to predict 'cases' at each interval was tested with a classifier employing an ensemble of weak-learners. In this Gradient Boosting method (Friedman, 2002), the cohort was split into a discrete training (75%) and validation (25%) set, employing 1000 trees with 10-fold cross-validation (R package *gbm*).

3. Results

3.1. Participant characteristics

The sample was predominantly male (18 females), predominantly middle-aged (mean age 61.7) with most patients being classified as the 'Akinetic-Rigid' (37.5%) or 'Mixed' phenotype (43.8%). Most patients

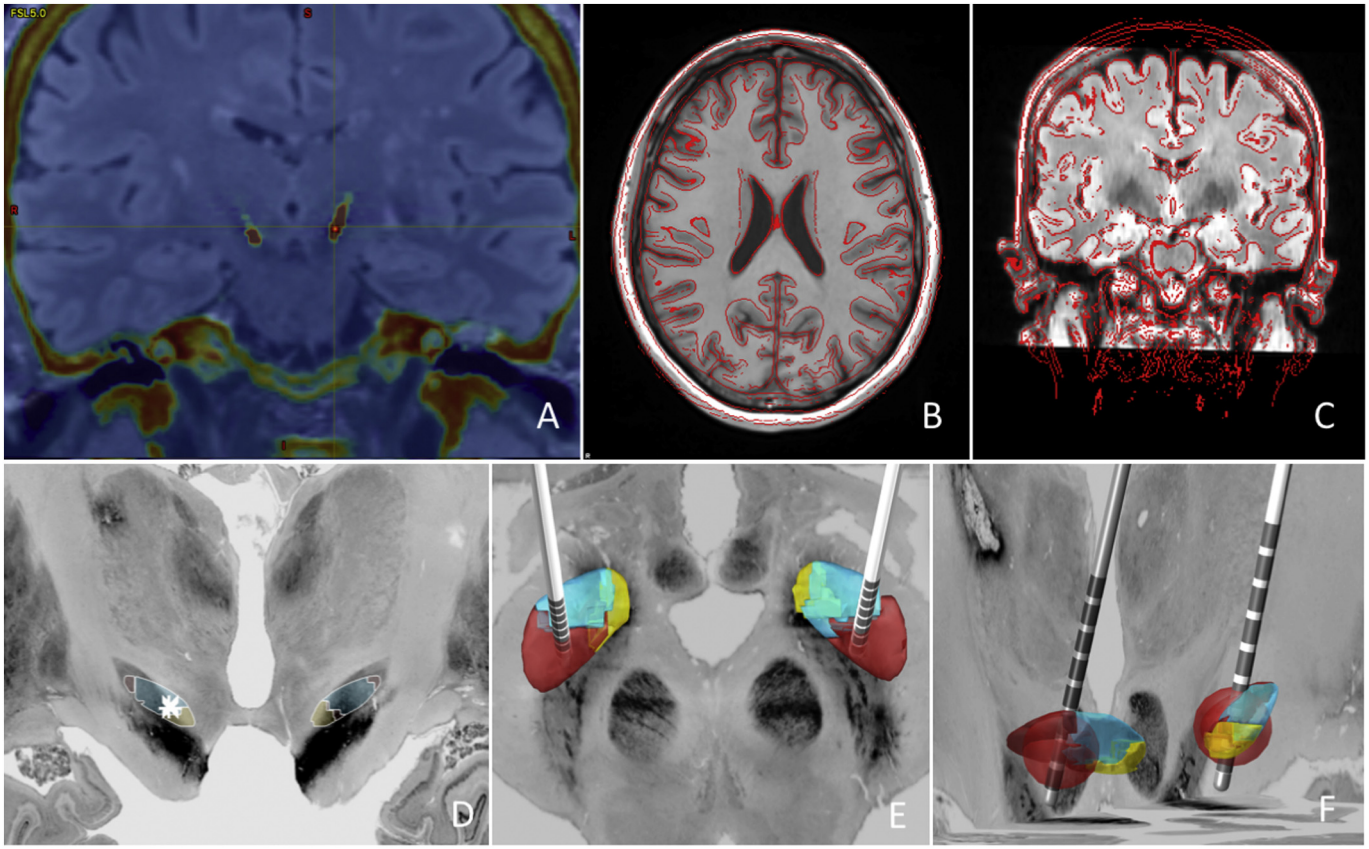

Fig. 2. Image processing pipeline for the identification of electrode contact points and volume activated tissue (VAT). A: MPRAGE, FLAIR and CT images were co-registered and manually checked for accuracy, with an accurately-sited electrode indexed in the right STN. B and C: Spatial normalisation into common template space using DARTEL. D: Coronal view of the active electrode contact (asterisk) with reference to the limbic (yellow), associative (blue) and motor (maroon) subregions of the STN. E: Axial view of both electrode trajectories with reference to the STN and its subregions. Within each STN limbic = yellow, associative = blue and motor = maroon subregions. F: Oblique sagittal view with simulated VAT in each hemisphere (red sphere). (For interpretation of the references to color in this figure legend, the reader is referred to the web version of this article.)

Table 1
Summary of the neuropsychiatric variables examined in this investigation; anatomical variables entered into the LASSO for regularisation and control variables entered into the general linear model.

Neuropsychiatric outcomes	Anatomical variables	GLM co-variates
Case versus non-case	*Distance to nearest voxel in each STN subregion:*	Age
Patient-rated BIS		Gender
Caregiver-rated BIS	*Distance to centroid of each STN subregion:*	Hoehn & Yahr stage
Patient-rated EQ	*Overlap of simulated VAT within each STN subregion:*	Clinical subtype
Caregiver-rated EQ		
QUIP-RS Including subscales (sex, gambling, eating etc.)	*Ratio of simulated VAT*: Right Associative:Motor STN Left Associative:Motor STN	Years since diagnosis
Beck depression inventory		LEDD
Hayling test Including: category A & B errors, AB error score		
ELF task Rule violations		

had moderate motor symptoms at baseline despite being 'ON' medication during UPDRS assessment. Summary statistics for these and selected neuropsychiatric variables are presented in Table 2.

3.2. Subthalamic stimulation

Analysis of the concatenated VAT volumes for the cohort demonstrated that the highest probability of stimulation was in the dorsolateral (motor) aspect of the STN, consistent with atlas-defined boundaries (Fig. 3). The only variable demonstrating a significant change between assessment intervals was an expected increase in stimulation amplitude (right hemisphere: 95% CI 0.17–0.58, $p = 0.0005$, left hemisphere: 95% CI 0.17–0.60, $p = 0.0005$; Supplementary Table 1). However, at each interval, some anatomical variables were significantly different between right and left hemispheres. At 6- and 13-weeks the active contact was closer to the centroid of the right associative subregion (6-weeks: 95% CI 0.53–1.40 mm, $p = 3.09 \times 10^{-4}$, 13-weeks: 95% CI 0.34–1.17 mm, $p = 0.006$), the nearest voxel of the right associative subregion (6-weeks: 95% CI 0.30–1.05 mm, $p = 0.0016$, 13-weeks: 95% CI 0.14–0.91 mm, $p = 0.026$) and the VAT occupation of the associative subregion was greater in the right hemisphere (6-weeks: 95% CI 5.89–19.99%, $p = 0.0016$, 13-weeks: 95% CI 3.17–18.2%, $p = 0.02$). At 6-weeks the active contact was also closer to the centroid of the right limbic subregion (95% CI 0.21–1.21 mm, $p = 0.0016$).

Table 2
Demographic and clinical characteristics of the study cohort at baseline:

Categorical variable	Total (n = 64)	
Gender	n	% total
Male	46	71.9
Female	18	28.1
Clinical subtype	n	% total
Akinetic-Rigid	24	37.5
Mixed	28	43.8
Tremor	12	18.8

Continuous variable	Mean (SD), median (range)
Age (years)	61.7 (± 9.3), 64 (35–76)
Hoehn & Yahr stage	2.7 (± 0.5), 2.5 (1.5–4)
Years since diagnosis	9.0 (± 5.2), 7 (1 – 23)
Levodopa equiv. daily dose	1077.3 (± 543.1), 1008 (0–3450)
Patient-rated BIS	60.6 (± 8.3), 60 (43–87)
Caregiver-rated BIS	59.4 (± 11.6), 59 (40–90)
Patient-rated EQ	42.6 (± 12.2), 42 (16–68)
Caregiver-rated EQ	38.9 (± 14.0), 42 (11–64)
QUIP-RS total	20.5 (± 15.0), 18 (0–63)
Beck depression inventory	11.1 (± 5.1) 11 (1 – 22)
Hayling AB error score	10.1 (± 11.2), 6 (0–45)
ELF rule violations	8.8 (± 5.4), 8 (0–24)
UPDRS part III motor	37.0 (± 16.6), 36 (10–91)

3.3. Neuropsychiatric outcomes

3.3.1. Assessment data

A repeated-measures ANOVA was employed to identify group-mean change amongst variables of interest across the chosen assessment intervals (baseline, 6-weeks and 13-weeks). As expected, there was a significant decrease in motor symptoms ($F = 10.38$, $p = 3.17 \times 10^{-4}$) and dopaminergic medication use ($F = 79.59$, $p = 2.4 \times 10^{-15}$) across the cohort. Controlling for age, gender, clinical subtype and dopaminergic medication use, this decrease in motor symptoms was related to the extent of the right subthalamic motor subregion occupied by the simulated VAT at 6-weeks ($p = 0.029$). At 13-weeks, by which time dopaminergic medication had been significantly reduced, raw scores on the UPDRS part III motor examination were also significantly associated with this anatomical variable ($p = 0.0098$). There were no other significant cohort-level longitudinal changes in neuropsychiatric variables that survived correction for false discovery rate. These complete data are presented in Supplementary Table 2.

We next sought to identify anatomical variables that were predictive of neuropsychiatric outcomes at follow-up assessments, as indexed by changes in scores from baseline. Greater ELF Rule Violations at both follow-up assessments were predicted by the extent to which the simulated VAT occupied the right associative STN subregion. When controlling for clinical and demographic factors, increased ELF rule violations were observed to be related to greater VAT overlap for the right associative STN subregion at both 6- ($t = 2.35$, $p = 0.023$) and 13-weeks ($t = 3.3$, $p = 0.0017$) (Table 3). The variable selection algorithm did not identify predictive anatomical variables for the other neuropsychiatric outcomes tested.

These findings were extended by identifying clusters of STN voxels significantly associated with ELF inhibitory errors. At both 6- and 13-weeks, clusters of subthalamic voxels in the right motor, as well as in the associative subregion, were significantly associated with an increase in inhibitory failure ($p < 0.05$, FWE-corrected) (Fig. 4). Cluster statistics are presented in Supplementary Table 7. Thresholded statistical maps (extracted with FSL randomise) corresponding to the significant cluster-based inferences of change in inhibitory errors are provided for download.

3.3.2. Clinical cases

A total of 26 participants were identified as cases (i.e. developed clinically-significant, stimulation-dependent changes in mood, affect and behaviour) during postoperative follow up. The characteristics of cases and non-cases were compared at baseline, 6-weeks and 13-weeks (Supplementary Tables 3–5). At baseline, in all demographic, disease-related and neuropsychiatric variables, there was no significant difference between groups (summarised in Supplementary Table 3). At the 6-week and 13-week assessments, there were no significant differences between cases and non-cases amongst the neuropsychiatric assessment data (summarised in Supplementary Tables 4 and 5). There were also no significant differences between groups in stimulation amplitude at either interval (left STN: $p = 0.54$ at 6 weeks and $p = 0.60$ at 13 weeks; right STN: $p = 0.29$ at 6-weeks and $p = 0.93$ at 13-weeks).

Anatomical variables with explanatory power were identified for caseness at both the 6-week and the 13-week assessments. These then also proved highly significant when controlling for clinical and demographic covariates. At 6-weeks, developing clinically-significant symptoms was significantly associated with stimulation at a closer distance to the nearest voxel of the right associative STN subregion ($z = -3.0$, $p = 0.0026$), as well as with greater VAT overlap within this subregion ($z = 3.31$, $p = 0.0009$). At 13-weeks, caseness was significantly associated with stimulation at a closer distance to the centroid of the right ($z = -3.0$, $p = 0.0027$) and left ($z = -2.63$, $p = 0.0084$) associative STN subregions, as well as with greater occupation of the right associative subregion by the simulated VAT ($z = 3.0$, $p = 0.0026$).

Clinical details of all identified cases are presented in Supplementary Table 6, including the stimulation manipulation undertaken to remit symptoms.

For each case, overlap of the left and right associative subregion by the simulated VAT was calculated pre- and post-intervention and tested for significant differences. This was repeated for the distance of the active electrode contact to the centroid of the associative subregion. Neuropsychiatric cases with active symptoms had a significantly greater volume of the right associative subthalamic subregion occupied by the simulated VAT than after remission of symptoms (95% CI 8.98–32.48%, $t = 3.54$, $p = 0.00087$). Likewise, neuropsychiatric cases with active symptoms had an active electrode contact significantly closer to the centroid of the right associative subthalamic subregion than after stimulation manipulation and remission of symptoms (95% CI 0.045–1.24 mm, $t = 2.17$, $p = 0.036$), although this finding did not survive FDR correction. Interestingly, these findings were not replicated in the left STN ($p = 0.15$ for VAT overlap of the left associative subregion and $p = 0.28$ for distance to the left associative centroid).

3.4. Predicting caseness from subthalamic data

A classifier applied to a training subset of the anatomical data showed broad agreement with the data acquired from the variable selection algorithm. In this classifier (Supplementary Fig. 2a and b), the overlap of the simulated VAT with the associative subregion of the right STN had the greatest explanatory power at both 6 and 13-weeks. At 6-weeks, this anatomical variable was the dominant factor in classification. At 13-weeks, the distance of the active electrode contact to the right and left associative subregions were also important factors, similar to the data presented in Table 4. Using iterative cross-validation the accuracy of the model at correctly classifying cases at 6-weeks was 79%

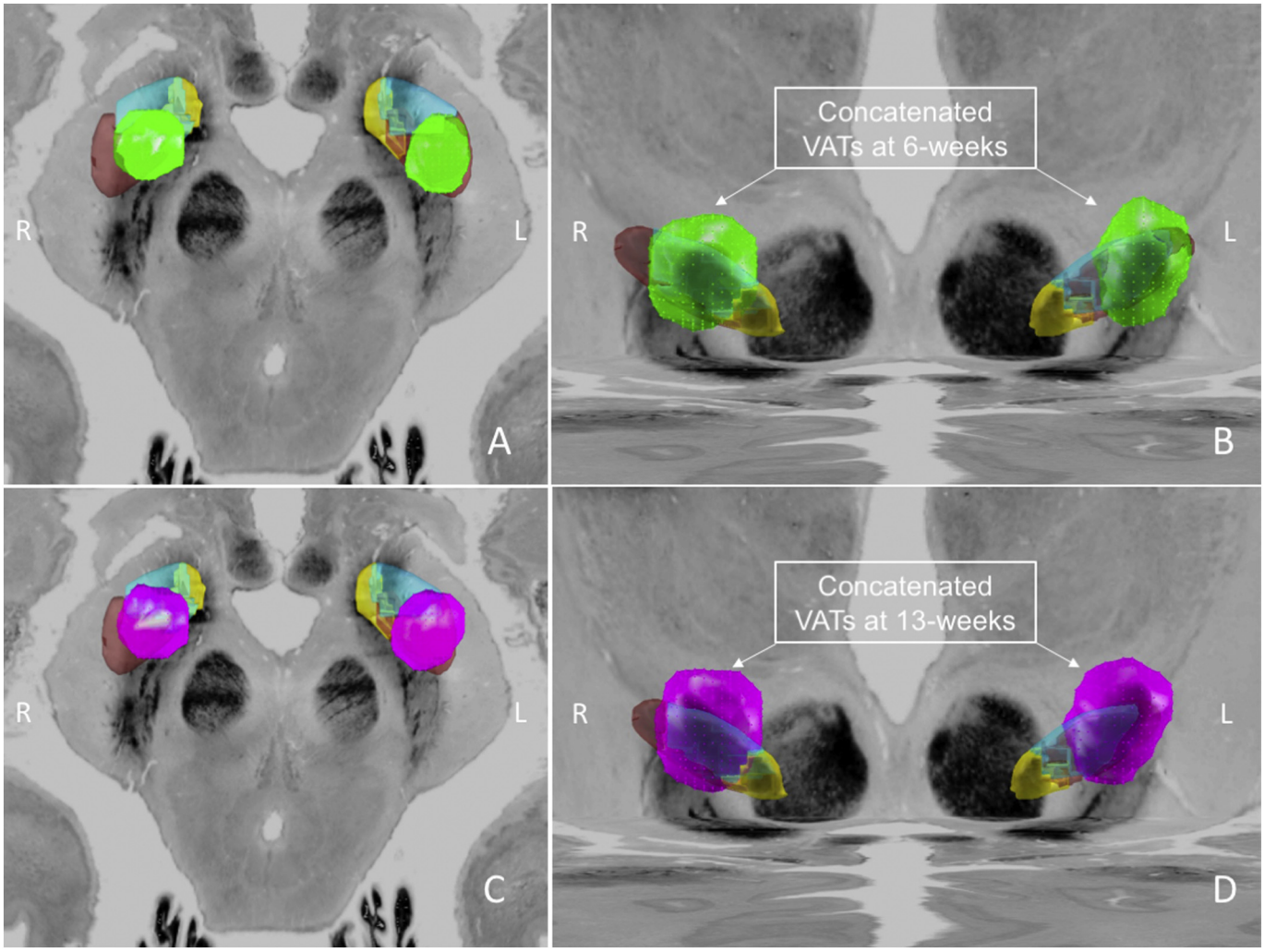

Fig. 3. Stimulation predominates in the dorsolateral aspect of the STN across the cohort. Hemispheric VATs for each participant were concatenated and thresholded to identify the highest frequency of overlapping voxels at 6-weeks (A and B) and 13-weeks (C and D). The subthalamic atlas is overlaid on a T2-weighted image in ICBM_2009b nonlinear asymmetric space. Within each STN limbic = yellow, associative = blue and motor = maroon subregions. A and C: Top 25% of overlapping voxels in the axial plane. B and D: Top 25% of overlapping voxels in the coronal plane. (For interpretation of the references to color in this figure legend, the reader is referred to the web version of this article.)

Table 3
Modelling of anatomical variables relating to neuropsychiatric assessment data. For each participant, standardised (z-scored) change values from baseline were calculated for each neuropsychiatric variable. These change scores were entered into a variable selection and optimisation algorithm to identify anatomical variables of interest. These anatomical variables were then tested in a general linear model, controlling for relevant disease and demographic factors.

ELF rule violations	Anatomical variables after optimisation	LASSO coefficients (fitted)	General linear model[a]
Week 6	VAT overlap: right associative STN	Intercept = −0.65 Coefficient = 0.0046	t-stat = 2.349 *p*-value = 0.023*
Week 13	VAT overlap: right associative STN	Intercept = −0.087 Coefficient = 0.0030	t-stat = 3.30 *p*-value = 0.0017**

Significance codes: '***' $p < 0.001$ '**' $p < 0.01$ '*' $p < 0.05$.
[a] Controlled for age, gender, LEDD, clinical subtype, years since diagnosis.

(*95% confidence interval 54.4–94.0*, *sensitivity 89%*, *specificity 70%*, *positive predictive value 73%*, *negative predictive value 89%*) and at 13-weeks was 79% (*95% confidence interval 54.4–94.0*, *sensitivity 71%*, *specificity 83%*, *positive predictive value 71%*, *negative predictive value 83%*).

The spatial distribution of STN voxels significantly associated with the likelihood of being a 'case' versus a 'non-case' were determined with a voxel-based analysis. The highest likelihood of being a 'case' and a 'non-case' was identified using the predicted probabilities of caseness in the machine-learning classifier trained on the whole dataset at 13-weeks (*accuracy 88%*, *95% confidence interval 76.9–94.5*, *sensitivity 90%*, *specificity 86%*, *positive predictive value 75%*, *negative predictive value 95%*). Distinct clusters of voxels were identified in the dorsolateral STN corresponding to the highest likelihood of being a 'non-case', with clusters of voxels in the ventromedial STN corresponding with the highest likelihood of being a 'case' (Fig. 5). Cluster Statistics are presented in Supplementary Table 7. Thresholded statistical maps (extracted with FSL randomise) corresponding to the significant cluster-based inferences of change in neuropsychiatric outcomes are provided for download.

3.5. Auxillary analyses

An additional analysis was carried out using scan group as an additional covariate for the significant findings detailed above. With the exception of ELF Rule Violations at 6-weeks post-DBS, all findings

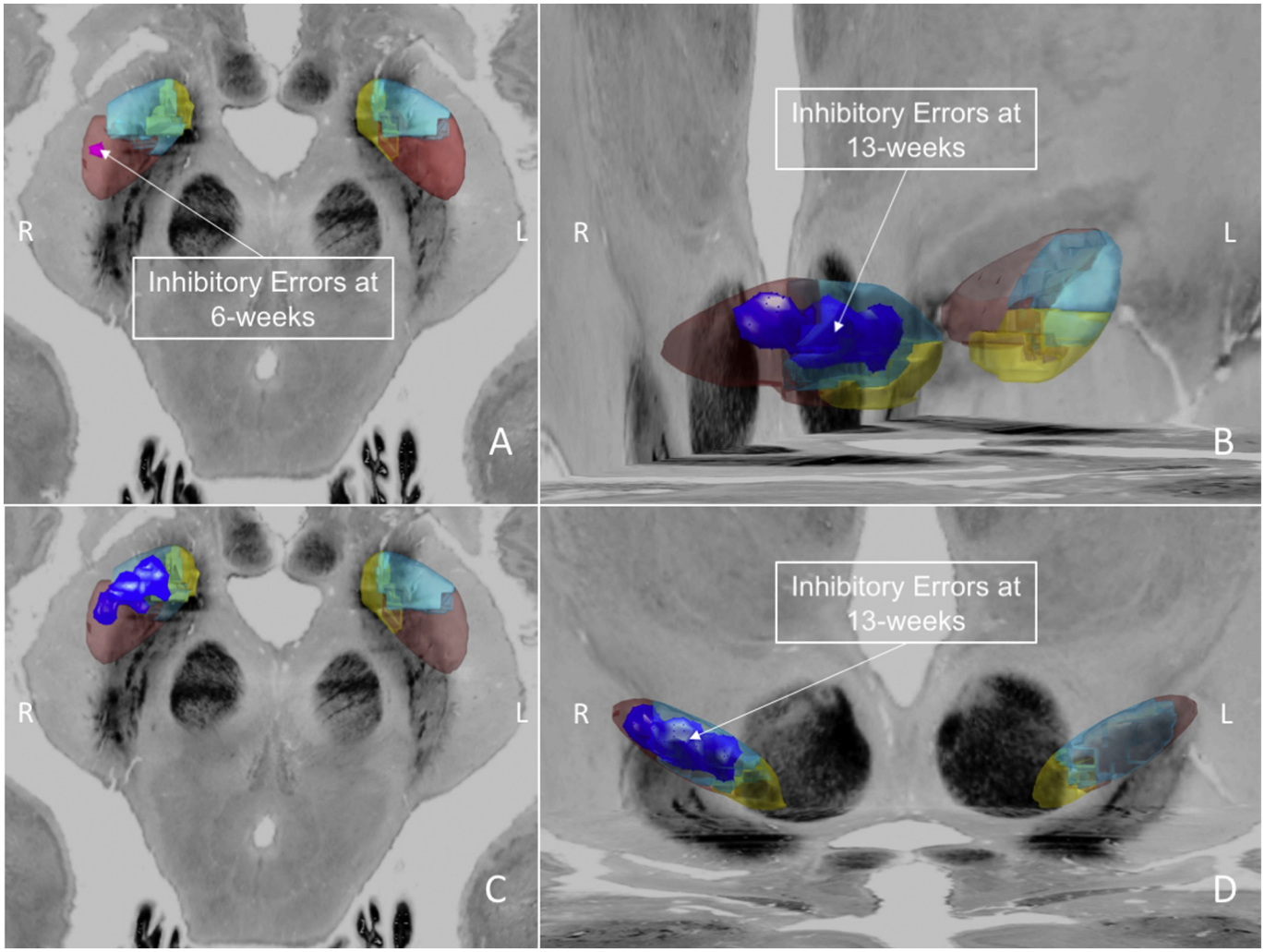

Fig. 4. Clusters of subthalamic voxels in the right associative and motor subregions are associated with inhibitory deficits 6- and 13-weeks after subthalamic DBS. Within each STN limbic = yellow, associative = blue and motor = maroon subregions. At 6-weeks, a small cluster of FWE-corrected subthalamic voxels significantly associated with ELF rule violations is observed in the right motor subregion (pink). At 13-weeks this cluster is larger and predominates in the right associative subregion, extending into the right motor subregion (blue). A: Axial view at 6-weeks, B: oblique view at 13-weeks, C: axial view at 13-weeks, D: coronal view at 13-weeks. (For interpretation of the references to color in this figure legend, the reader is referred to the web version of this article.)

remained significant (Supplementary Table 8), indicating that these findings are replicated across scanning conditions. Furthermore, we repeated the main analyses using the recently released DISTAL subthalamic atlas, which is precisely co-registered to the ICBM nonlinear asymmetric MNI space and includes limbic, associative and motor subregions. Our findings were replicated in this atlas (Supplementary Table 9).

4. Discussion

We demonstrate the significance of the locus of subthalamic stimulation in the genesis of postoperative inhibitory dysfunction. We found that the spatial overlap between the inferred stimulation volume and the associative subregion of the right STN was significantly associated with inhibitory errors during the Excluded Letter Fluency (ELF) task. Rule violations in this task are a sensitive measure of inhibitory dysfunction in non-demented persons with Parkinson's disease and are considered to represent goal-directed, selective inhibitory control. It may be a more sensitive measure of disinhibition than the Hayling sentence completion task in this population (O'Callaghan et al., 2013). We found a cluster of subthalamic voxels in the right STN associated with greater ELF rule-violations at 6 and 13-weeks post-DBS. The inclusion of motor and associative zones in these clusters emphasises that the partitioning of STN subregions is not strictly delineated and is more likely to be represented by a gradient of sensorimotor-cognitive cortical connectivity.

We also demonstrate that clinically-significant, stimulation-dependent neuropsychiatric symptoms (changes in mood, affect and behaviour from baseline, as assessed by a psychiatrist, responding immediately to stimulation manipulation) are also associated with the spatial overlap of the simulated VAT in the right associative STN, as well as the distance of the active contact from the nearest voxel of the associative subregion, and the centroid of the right and left associative subregions. We identify distinct clusters of voxels associated with high and low likelihood of stimulation-dependent neuropsychiatric symptoms and illustrate that postoperative 'cases' can be predicted with reasonable accuracy from these methods.

Our investigation adds to the literature in the following ways. By using a larger sample size than many recent investigations, we were able to infer more accurately on the contribution of subthalamic stimulation to neuropsychiatric outcome. Secondly, our neuropsychiatric evaluation pre- and post-DBS was extensive and allowed us to discriminate between clinically-significant syndromes (such as mania and hypomania) and subclinical changes in dimensional constructs (such as

Table 4
Modelling of anatomical variables relating to clinical caseness after subthalamic DBS. Neuropsychiatric 'cases' were identified based on an operationalised assessment schedule by a psychiatrist. The factor 'case' versus 'non-case' was entered into a variable selection and optimisation algorithm to identify anatomical variables of interest. These anatomical variables were then tested in a general linear model, controlling for relevant disease and demographic factors.

Clinical cases	Anatomical variables after optimisation	LASSO coefficients (fitted)	General linear model[a]
Week 6	Distance: right associative STN voxel	Intercept = −0.72 Coefficient = −0.11	z-value = −3.00 *p*-value = 0.0026**
	VAT overlap: right associative STN	Intercept = −0.72 Coefficient = 0.016	z-value = 3.31 *p*-value = 0.0009***
Week 13	Distance: right associative STN centroid	Intercept = 0.19 Coefficient = −0.29	z-value = −3.00 *p*-value = 0.0027**
	Distance: left associative STN centroid	Intercept = 0.19 Coefficient = −0.049	z-value = −2.63 *p*-value = 0.0084**
	VAT overlap: right associative STN	Intercept = 0.19 Coefficient = 0.0046	z-value = 3.00 *p*-value = 0.0026**

Significance codes: '***' $p < 0.001$ '**' $p < 0.01$ '*' $p < 0.05$.
[a] Controlled for age, gender, LEDD, clinical subtype, years since diagnosis.

impulsivity). Thirdly, by employing a voxel-wise analysis of the STN, we were able to report more detailed information about regions likely to be associated with neuropsychiatric impairment. Finally, we applied classification techniques to our dataset to quantify the ability of this information to predict clinical outcomes.

We acknowledge several limitations of our approach. Firstly, the precise boundaries and orientation of the STN may display inter-subject heterogeneity, which introduces a potential source of error when using an atlas developed in a non-surgical population. However, accurate manual segmentation of the STN using standard acquisitions at 3-Tesla is challenging, prone to inter-rater variability and additional data, such as the functional topography of the nucleus, is lost. We addressed this concern by deforming individual acquisitions to a common space, but recognise that a bias may persist given that the subthalamic atlas was not defined in the space used for nonlinear warps (Ewert et al., 2017). This could introduce a systematic bias in the subsequent analysis of subthalamic volumes. However, we repeated our main analyses using the recently released DISTAL subthalamic atlas, which is precisely co-registered to the ICBM nonlinear asymmetric MNI space (Ewert et al., 2017). All findings remained statistically significant, again weighted toward the right over the left STN. Furthermore, our finding that the topmost 25% of overlapping voxels in our group VAT volume overlay the motor territory of the STN in both hemispheres lends plausibility to our approach and suggests any errors induced by normalisation to a common space were not excessive, with electrode targeting and DBS programming most likely to eventuate in stimulation of the motor subregion of this nucleus.

We have also used a simplified method for estimating each VAT, which fails to account for tissue inhomogeneity and the biophysics of axonal response to DBS (Gunalan et al., 2017). However, the methods we employ benefit from being embedded in open-source rather than proprietary software and are not computationally demanding to implement.

The use of two different MRI scanners for image acquisition introduces a further variable, but the acquisition protocol was not altered and we present key data from our analyses controlling for scan group in Supplementary Table 7. Overall, the correlation of anatomical variables with inhibitory deficits and neuropsychiatric 'caseness', derived from the general linear model, remains highly significant despite this additional covariate. The sole exception is ELF rule violations at 6-weeks, which is no longer significantly correlated with VAT overlap within the right associative subthalamic subregion. This was the finding of weakest significance in the original analysis. However, that the remaining results hold despite the addition of scan group to the model, arguably increases the generalisability of our findings.

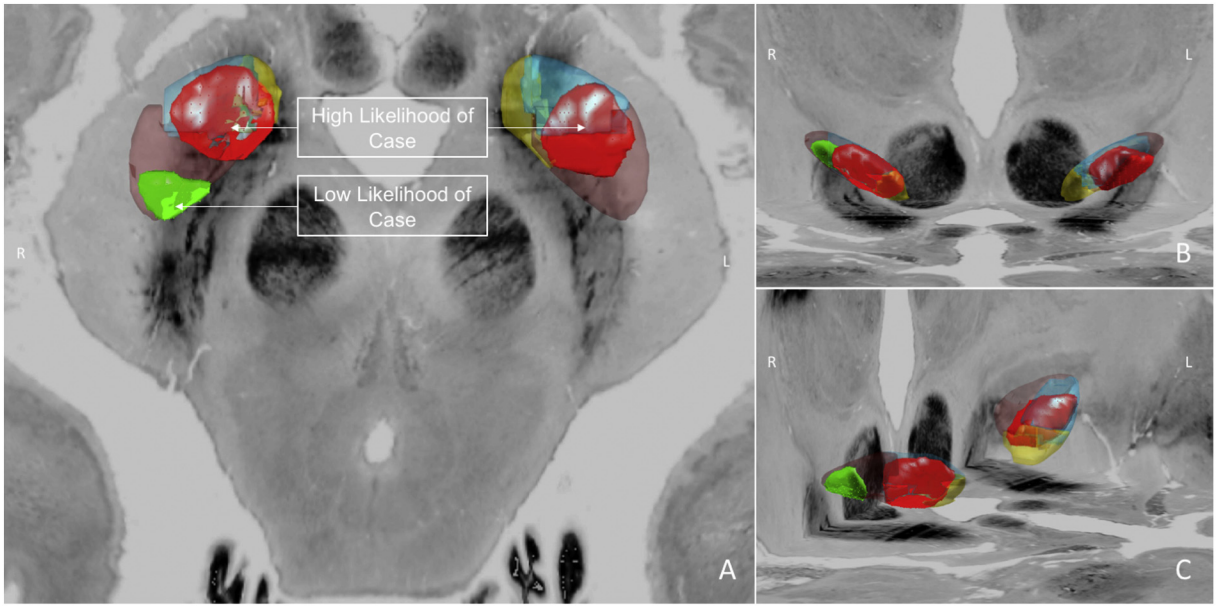

Fig. 5. Distinct clusters of subthalamic voxels are associated with high and low likelihood of developing clinically-significant neuropsychiatric symptoms after STN-DBS for Parkinson's disease. Within each STN limbic = yellow, associative = blue and motor = maroon subregions. Green: a cluster of FWE-corrected voxels significantly associated with being a non-case can be identified in the dorsolateral aspect of the right STN. Red: a cluster of FWE-corrected voxels significantly associated with being a case are identified in the ventromedial aspect of both the right and left STN. Significant clusters are found in both the right and left STN, corresponding with the known anatomy of this nucleus, with motor representations in the dorsolateral aspect of this nucleus and cognitive-associative circuits in the ventromedial region. A: Axial view, B: Coronal view, C: Oblique view. (For interpretation of the references to color in this figure legend, the reader is referred to the web version of this article.)

The proportion of neuropsychiatric 'cases' in our investigation (40%) is significantly higher than that reported in previous work (Voon et al., 2006). However, we emphasise that our definition of 'caseness' did not require participants to meet criteria for a full manic episode. Rather, isolated symptoms such as impulsive decision-making or verbal disinhibition met our criteria, providing they arose de novo during stimulation titration, responded to stimulation manipulation and, whilst present, caused significant personal or relational distress. Formal pre- and postoperative psychiatric assessment within the movement disorders centre likely enhanced sensitivity to detect attenuated symptoms. We also note that 43.5% of caregivers in a recent investigation endorsed a negative postoperative 'personality change' in their partners (Lewis et al., 2014). It is challenging to robustly operationalise this construct, but we argue that our criteria of linking symptom resolution with stimulation manipulation, as well as seeking collateral information from third parties, increases the reliability of assignment to the 'case' category.

Aside from the ELF, no other anatomical variables showed explanatory power for other neuropsychiatric assessment instruments. This may also represent the reduced sensitivity of other instruments to change, as well as the complex role of other factors such as LEDD reduction and reduced participant insight into behavioural symptoms.

Although our significant findings were biased to the right hemisphere, we cannot draw definitive conclusions regarding the laterality of any aetiologic mechanism, given the presence of significant interhemispheric differences between relevant associative and limbic variables (see Supplementary Table 1). However, this finding is intriguing, given previous work suggesting that executive control of inhibition is primarily a right-lateralised process (Aron et al., 2004; D'Alberto et al., 2017; Possin et al., 2009). The STN forms a key node in a right-hemispheric network incorporating the Inferior Frontal Gyrus and the pre-Supplementary Motor Area, which subserves slowing and inhibition following the detection of cognitive conflict (Aron et al., 2007). This function is mediated through activation of the STN via the hyperdirect pathway, with the efficiency of inhibition correlated with the connectivity between these right-hemispheric nodes (Rae et al., 2015). Therefore, it is plausible that neurostimulation of the right STN in our subjects is more likely to induce disinhibition and suggests that the right hemisphere might be the first site to target when addressing stimulation-induced neuropsychiatric symptoms.

4.1. Conclusions

In sum, we have found empirical support for the hypothesised link between the site of subthalamic stimulation and the emergence of postoperative neuropsychiatric symptoms after STN-DBS for Parkinson's disease. By simulating a volume of activated tissue for each participant, we were able to represent additional information about the spread of charge from the active electrode contact. Consistent with the known gradient of cortical representations within the STN, we demonstrated a connection between the associative subregion and postoperative disinhibition, in addition to the emergence of clinically-significant neuropsychiatric symptoms. Across the whole STN, we were able to delineate distinct clusters of voxels associated with inhibitory impairment, as well as the likelihood of neuropsychiatric 'caseness'. Classification methods applied to our data were able to classify 'cases' with reasonable accuracy. Our findings suggest that electrode targeting within the STN and stimulation diffusion within more ventromedial aspects of this nucleus does have an important role in mediating neuropsychiatric outcome. This extends previous work on the importance of electrode targeting and stimulation titration for optimal motor outcome and corroborates existing data on the functional anatomy of this nucleus, derived from non-human primates and neuroimaging data in healthy subjects. We anticipate that data such as these could be used prospectively to guide DBS titration and enhance the safety profile of this clinically-effective therapy.

Recently, several groups have employed diffusion imaging to characterise the connectivity profile of clinically-effective subthalamic stimulation (Accolla et al., 2016; Akram et al., 2017; Horn et al., 2017; Vanegas-Arroyave et al., 2016), although neuropsychiatric symptoms have not been formally examined in these approaches. Tractographic methods are able to incorporate white matter tracts adjacent to the STN, which may contribute to the balance of therapeutic versus adverse effects. Models of neural networks associated with favourable clinical outcomes offer insights into the mechanism of DBS and may, in the future, assist clinicians with selection of the optimal electrode contact and guide stimulation titration. Future work will evaluate if diffusion imaging surpasses other forms of data when predicting the evolution of postoperative neuropsychiatric symptoms.

Supplementary data to this article can be found online at https://doi.org/10.1016/j.nicl.2018.03.009.

Acknowledgements

The authors gratefully acknowledge the commitment of participants and caregivers who contributed their time to this study. The authors acknowledge the ongoing support of St Andrew's War Memorial Hospital and the Herston Imaging Research Facility. The authors thank the Lead-DBS developers for providing an open-source platform for the analysis of deep brain stimulation data.

Financial disclosures/conflicts of interest

All authors report no conflict of interest.

Funding agencies

Dr Mosley was supported by an early career fellowship from the Queensland government's 'Advance Queensland' initiative, a Royal Brisbane & Woman's Hospital Foundation Research Grant and a young investigator grant from the Royal Australian and New Zealand College of Psychiatrists. He received an unrestricted educational grant from Medtronic.

Ethics approval

Prior to the commencement of data collection, the full protocol was approved by the Human Research Ethics Committees of the Royal Brisbane & Women's Hospital, the University of Queensland, the QIMR Berghofer Medical Research Institute and UnitingCare Health. All participants and caregivers gave written consent to participate in the study.

Author roles

Mosley: Conception and design of study, data collection, writing the first draft of the manuscript, image processing and analysis, statistical analysis.

Smith: Statistical supervision.

Coyne: Supervision of data collection, critical comments on manuscript.

Silburn: Supervision of data collection, critical comments on manuscript.

Breakspear: Supervision of study design, analytical methods and revision of manuscript.

Perry: Design and supervision of image processing and analysis, statistical analysis, revision of manuscript.

References

Accolla, E.A., Dukart, J., Helms, G., Weiskopf, N., Kherif, F., Lutti, A., et al., 2014. Brain tissue properties differentiate between motor and limbic basal ganglia circuits. Hum. Brain Mapp. 35, 5083–5092.

Accolla, E.A., Herrojo Ruiz, M., Horn, A., Schneider, G.H., Schmitz-Hubsch, T., Draganski, B., et al., 2016. Brain networks modulated by subthalamic nucleus deep brain stimulation. Brain 139, 2503–2515.

Akram, H., Sotiropoulos, S.N., Jbabdi, S., Georgiev, D., Mahlknecht, P., Hyam, J., et al., 2017. Subthalamic deep brain stimulation sweet spots and hyperdirect cortical connectivity in Parkinson's disease. NeuroImage 158, 332–345.
Alkemade, A., Forstmann, B.U., 2014. Do we need to revise the tripartite subdivision hypothesis of the human subthalamic nucleus (STN)? NeuroImage 95, 326–329.
Amunts, K., Lepage, C., Borgeat, L., Mohlberg, H., Dickscheid, T., Rousseau, M.E., Bludau, S., Bazin, P.L., Lewis, L.B., Oros-Peusquens, A.M., Shah, N.J., Lippert, T., Zilles, K., Evans, A.C., 2013. BigBrain: An ultrahigh-resolution 3D human brain model. Science 340 (6139), 1472–1475.
Appleby, B.S., Duggan, P.S., Regenberg, A., Rabins, P.V., 2007. Psychiatric and neuropsychiatric adverse events associated with deep brain stimulation: a meta-analysis of ten years' experience. Mov. Disord. 22, 1722–1728.
Aron, A.R., Robbins, T.W., Poldrack, R.A., 2004. Inhibition and the right inferior frontal cortex. Trends Cogn. Sci. 8, 170–177.
Aron, A.R., Behrens, T.E., Smith, S., Frank, M.J., Poldrack, R.A., 2007. Triangulating a cognitive control network using diffusion-weighted magnetic resonance imaging (MRI) and functional MRI. J. Neurosci. 27, 3743–3752.
Ashburner, J., 2007. A fast diffeomorphic image registration algorithm. NeuroImage 38, 95–113.
Baron-Cohen, S., Wheelwright, S., 2004. The empathy quotient: an investigation of adults with Asperger syndrome or high functioning autism, and normal sex differences. J. Autism Dev. Disord. 34, 163–175.
Beck, A.T., Ward, C.H., Mendelson, M., Mock, J., Erbaugh, J., 1961. An inventory for measuring depression. Arch. Gen. Psychiatry 4, 561–571.
Benjamini, Y., Hochberg, Y., 1995. Controlling the false discovery rate: a practical and powerful approach to multiple testing. J. R. Stat. Soc. Ser. B Methodol. 57, 289–300.
Burgess, P.W., Shallice, T., Thames Valley Test Company, 1997. The Hayling and Brixton Tests. Vol.. Thames Valley Test Company, Bury St Edmunds.
van Buuren, S., Groothuis-Oudshoorn, K., 2011. mice: multivariate imputation by chained equations in R. J. Stat. Softw. 45.
Cavanagh, J.F., Wiecki, T.V., Cohen, M.X., Figueroa, C.M., Samanta, J., Sherman, S.J., et al., 2011. Subthalamic nucleus stimulation reverses mediofrontal influence over decision threshold. Nat. Neurosci. 14, 1462–1467.
D'Alberto, N., Funnell, M., Potter, A., Garavan, H., 2017. A split-brain case study on the hemispheric lateralization of inhibitory control. Neuropsychologia 99, 24–29.
Daniele, A., Albanese, A., Contarino, M.F., Zinzi, P., Barbier, A., Gasparini, F., et al., 2003. Cognitive and behavioural effects of chronic stimulation of the subthalamic nucleus in patients with Parkinson's disease. J. Neurol. Neurosurg. Psychiatry 74, 175–182.
Emre, M., Aarsland, D., Brown, R., Burn, D.J., Duyckaerts, C., Mizuno, Y., et al., 2007. Clinical diagnostic criteria for dementia associated with Parkinson's disease. Mov. Disord. 22, 1689–1707 (quiz 1837).
Evans, A.H., Katzenschlager, R., Paviour, D., O'Sullivan, J.D., Appel, S., Lawrence, A.D., et al., 2004. Punding in Parkinson's disease: its relation to the dopamine dysregulation syndrome. Mov. Disord. 19, 397–405.
Ewert, S., Plettig, P., Li, N., Chakravarty, M.M., Collins, D.L., Herrington, T.M., et al., 2017. Toward defining deep brain stimulation targets in MNI space: a subcortical atlas based on multimodal MRI, histology and structural connectivity. NeuroImage. http://dx.doi.org/10.1016/j.neuroimage.2017.05.015.
Frank, M.J., Samanta, J., Moustafa, A.A., Sherman, S.J., 2007. Hold your horses: impulsivity, deep brain stimulation, and medication in Parkinsonism. Science 318, 1309–1312.
Friedman, J.H., 2002. Stochastic gradient boosting. Comput. Stat. Data Anal. 38, 367–378.
Friedman, J., Hastie, T., Tibshirani, R., 2010. Regularization paths for generalized linear models via coordinate descent. J. Stat. Softw. 33, 1–22.
Gunalan, K., Chaturvedi, A., Howell, B., Duchin, Y., Lempka, S.F., Patriat, R., et al., 2017. Creating and parameterizing patient-specific deep brain stimulation pathway-activation models using the hyperdirect pathway as an example. PLoS One 12, e0176132.
Hastie, T., Tibshirani, R., Friedman, J.H., 2009. The Elements of Statistical Learning : Data Mining, Inference, and Prediction. Vol.. Springer, New York, NY.
Haynes, W.I., Haber, S.N., 2013. The organization of prefrontal-subthalamic inputs in primates provides an anatomical substrate for both functional specificity and integration: implications for Basal Ganglia models and deep brain stimulation. J. Neurosci. 33, 4804–4814.
Hershey, T., Revilla, F.J., Wernle, A., Gibson, P.S., Dowling, J.L., Perlmutter, J.S., 2004. Stimulation of STN impairs aspects of cognitive control in PD. Neurology 62, 1110–1114.
Hershey, T., Campbell, M.C., Videen, T.O., Lugar, H.M., Weaver, P.M., Hartlein, J., et al., 2010. Mapping Go-No-Go performance within the subthalamic nucleus region. Brain 133, 3625–3634.
Hoehn, M.M., Yahr, M.D., 1967. Parkinsonism: onset, progression and mortality. Neurology 17, 427–442.
Horn, A., Kuhn, A.A., 2015. Lead-DBS: a toolbox for deep brain stimulation electrode localizations and visualizations. NeuroImage 107, 127–135.
Horn, A., Reich, M., Vorwerk, J., Li, N., Wenzel, G., Fang, Q., et al., 2017. Connectivity predicts deep brain stimulation outcome in Parkinson disease. Ann. Neurol. 82, 67–78.
Hughes, A.J., Daniel, S.E., Kilford, L., Lees, A.J., 1992. Accuracy of clinical diagnosis of idiopathic Parkinson's disease: a clinico-pathological study of 100 cases. J. Neurol. Neurosurg. Psychiatry 55, 181–184.
Lambert, C., Zrinzo, L., Nagy, Z., Lutti, A., Hariz, M., Foltynie, T., et al., 2012. Confirmation of functional zones within the human subthalamic nucleus: patterns of connectivity and sub-parcellation using diffusion weighted imaging. NeuroImage 60, 83–94.
Lambert, C., Zrinzo, L., Nagy, Z., Lutti, A., Hariz, M., Foltynie, T., et al., 2015. Do we need to revise the tripartite subdivision hypothesis of the human subthalamic nucleus (STN)? Response to Alkemade and Forstmann. NeuroImage 110, 1–2.
Lewis, C.J., Maier, F., Horstkötter, N., Zywczok, A., Witt, K., Eggers, C., et al., 2014. Subjectively perceived personality and mood changes associated with subthalamic stimulation in patients with Parkinson's disease. Psychol. Med. 1–13. http://dx.doi.org/10.1017/s0033291714001081.
Lewis, C.J., Maier, F., Horstkotter, N., Eggers, C., Visser-Vandewalle, V., Moro, E., et al., 2015. The impact of subthalamic deep brain stimulation on caregivers of Parkinson's disease patients: an exploratory study. J. Neurol. 262, 337–345.
Madler, B., Coenen, V.A., 2012. Explaining clinical effects of deep brain stimulation through simplified target-specific modeling of the volume of activated tissue. AJNR Am. J. Neuroradiol. 33, 1072–1080.
Mallet, L., Schupbach, M., N'Diaye, K., Remy, P., Bardinet, E., Czernecki, V., et al., 2007. Stimulation of subterritories of the subthalamic nucleus reveals its role in the integration of the emotional and motor aspects of behavior. Proc. Natl. Acad. Sci. U. S. A. 104, 10661–10666.
Mosley, P.E., Marsh, R., 2015. The psychiatric and neuropsychiatric symptoms after subthalamic stimulation for Parkinson's disease. J. Neuropsychiatr. Clin. Neurosci. 27, 19–26.
Mosley, P.E., Breakspear, M., Coyne, T., Silburn, P.A., Smith, D., 2018. Caregiver burden and caregiver appraisal of psychiatric symptoms are not modulated by subthalamic deep brain stimulation for Parkinson's disease. npj Parkinson Dis in press.
Nambu, A., Tokuno, H., Takada, M., 2002. Functional significance of the cortico-subthalamo-pallidal 'hyperdirect' pathway. Neurosci. Res. 43, 111–117.
Obeso, I., Wilkinson, L., Rodriguez-Oroz, M.C., Obeso, J.A., Jahanshahi, M., 2013. Bilateral stimulation of the subthalamic nucleus has differential effects on reactive and proactive inhibition and conflict-induced slowing in Parkinson's disease. Exp. Brain Res. 226, 451–462.
O'Callaghan, C., Naismith, S.L., Shine, J.M., Bertoux, M., Lewis, S.J., Hornberger, M., 2013. A novel bedside task to tap inhibitory dysfunction and fronto-striatal atrophy in Parkinson's disease. Parkinsonism Relat. Disord. 19, 827–830.
Patton, J.H., Stanford, M.S., Barratt, E.S., 1995. Factor structure of the Barratt impulsiveness scale. J. Clin. Psychol. 51, 768–774.
Possin, K.L., Brambati, S.M., Rosen, H.J., Johnson, J.K., Pa, J., Weiner, M.W., et al., 2009. Rule violation errors are associated with right lateral prefrontal cortex atrophy in neurodegenerative disease. J. Int. Neuropsychol. Soc. 15, 354–364.
R Core Team, 2014. R: A Language and Environment for Statistical Computing. Vol.. R Foundation for Statistical Computing. Vienna, Austria.
Rae, C.L., Hughes, L.E., Anderson, M.C., Rowe, J.B., 2015. The prefrontal cortex achieves inhibitory control by facilitating subcortical motor pathway connectivity. J. Neurosci. 35, 786–794.
Schuepbach, W.M., Rau, J., Knudsen, K., Volkmann, J., Krack, P., Timmermann, L., et al., 2013. Neurostimulation for Parkinson's disease with early motor complications. N. Engl. J. Med. 368, 610–622.
Schupbach, M., Gargiulo, M., Welter, M.L., Mallet, L., Behar, C., Houeto, J.L., et al., 2006. Neurosurgery in Parkinson disease: a distressed mind in a repaired body? Neurology 66, 1811–1816.
Seymour, B., Barbe, M., Dayan, P., Shiner, T., Dolan, R., Fink, G.R., 2016. Deep brain stimulation of the subthalamic nucleus modulates sensitivity to decision outcome value in Parkinson's disease. Sci. Rep. 6, 32509.
Shores, E.A., Carstairs, J.R., Crawford, J.R., 2006. Excluded Letter Fluency Test (ELF): norms and test–retest reliability data for healthy young adults. In: Brain Impairment. 7. pp. 26–32.
Smith, S.M., Nichols, T.E., 2009. Threshold-free cluster enhancement: addressing problems of smoothing, threshold dependence and localisation in cluster inference. NeuroImage 44, 83–98.
Smith, S.M., Jenkinson, M., Woolrich, M.W., Beckmann, C.F., Behrens, T.E., Johansen-Berg, H., et al., 2004. Advances in functional and structural MR image analysis and implementation as FSL. NeuroImage 23 (Suppl. 1), S208–19.
Spiegel, J., Hellwig, D., Samnick, S., Jost, W., Mollers, M.O., Fassbender, K., et al., 2007. Striatal FP-CIT uptake differs in the subtypes of early Parkinson's disease. J. Neural Transm. 114, 331–335.
Thobois, S., Hotton, G.R., Pinto, S., Wilkinson, L., Limousin-Dowsey, P., Brooks, D.J., et al., 2007. STN stimulation alters pallidal-frontal coupling during response selection under competition. J. Cereb. Blood Flow Metab. 27, 1173–1184.
Vanegas-Arroyave, N., Lauro, P.M., Huang, L., Hallett, M., Horovitz, S.G., Zaghloul, K.A., et al., 2016. Tractography patterns of subthalamic nucleus deep brain stimulation. Brain 139, 1200–1210.
Voon, V., Kubu, C., Krack, P., Houeto, J.L., Troster, A.I., 2006. Deep brain stimulation: neuropsychological and neuropsychiatric issues. Mov. Disord. 21 (Suppl. 14), S305–27.
Weintraub, D., Burn, D.J., 2011. Parkinson's disease: the quintessential neuropsychiatric disorder. Mov. Disord. 26, 1022–1031.
Weintraub, D., Mamikonyan, E., Papay, K., Shea, J.A., Xie, S.X., Siderowf, A., 2012. Questionnaire for impulsive-compulsive disorders in Parkinson's Disease–Rating Scale. Mov. Disord. 27, 242–247.
Welter, M.L., Schupbach, M., Czernecki, V., Karachi, C., Fernandez-Vidal, S., Golmard, J.L., et al., 2014. Optimal target localization for subthalamic stimulation in patients with Parkinson disease. Neurology 82, 1352–1361.
Winkler, A.M., Ridgway, G.R., Webster, M.A., Smith, S.M., Nichols, T.E., 2014. Permutation inference for the general linear model. NeuroImage 92, 381–397.
Witt, K., Pulkowski, U., Herzog, J., Lorenz, D., Hamel, W., Deuschl, G., et al., 2004. Deep brain stimulation of the subthalamic nucleus improves cognitive flexibility but impairs response inhibition in Parkinson disease. Arch. Neurol. 61, 697–700.
Wodarg, F., Herzog, J., Reese, R., Falk, D., Pinsker, M.O., Steigerwald, F., et al., 2012. Stimulation site within the MRI-defined STN predicts postoperative motor outcome. Mov. Disord. 27, 874–879.